33rd Annual International Conference of the IEEE EMBS
Boston, Massachusetts USA, August 30 - September 3, 2011

Improving vessel segmentation in ultra-wide field-of-view retinal fluorescein angiograms

A. Perez-Rovira, K. Zutis, J.P. Hubschman and E. Trucco

***Abstract*— Vessel segmentation on ultra-wide field-of-view fluorescein angiogram sequences of the retina is a challenging problem. Vessel appearance undergoes severe changes, as different portions of the vascular structure become perfused in different frames. This paper presents a method for segmenting vessels in such sequences using steerable filters and automatic thresholding. We introduce a penalization stage on regions with high vessel response in the filtered image, improving the detection of peripheral vessels and reducing false positives around the optic disc and in regions of choroidal vessels and lesions. Quantitative results are provided, in which the penalization stage improves the segmentation precision segmentation by 11.84%, the recall by 12.98% and the accuracy by 0.40%. To facilitate further evaluation, usage, and algorithm comparison, the algorithm, the data set used, the ground truth, and the results are made available on the internet.**

I. Introduction

This paper presents a vessel segmentation algorithm for ultra-wide-field-of-view (UWFV) fluorescein angiograms (FA) sequences of the retina, based on the enhancement of ridge-like structures, penalization of areas with high vessel response and automatic thresholding for the final binarization.

Recent developments of scanning laser ophthalmoscopes (SLO) have made UWFV angiographic images possible, providing a new method to visualize up to 200° of the retina (conventional fundus cameras afford a field of view of about $30^\circ - 50^\circ$). This technology is becoming increasingly common and improving constantly [1]. Recent publications have clearly demonstrated that UWFV angiography provides visualization of peripheral retinal lesions and is useful in their evaluation and treatment [2].

FA sequences involve the intravenous administration of a fluorescein dye. Different portions of the vasculature become visible at different times, as the dye passes through the vascular system. Figure 1 shows frames from the 4 stages of a FA sequence: *arterial*, *arterio-venous*, *venous* and *late venous*. Sequence frames are not registered due to head and eye movements and mobile hardware components.

Numerous methods have been published on retinal vessel segmentation. The majority of methods focus on fundus images [3], [4], and only a few seem to have targeted FA [5], [6]. To the authors best knowledge, only a small number of simple techniques have been reported to extract vessel structures from UWFV FA sequences [7], [8], and no specialized vessel segmentation system for UWFV FA images has been evaluated quantitatively.

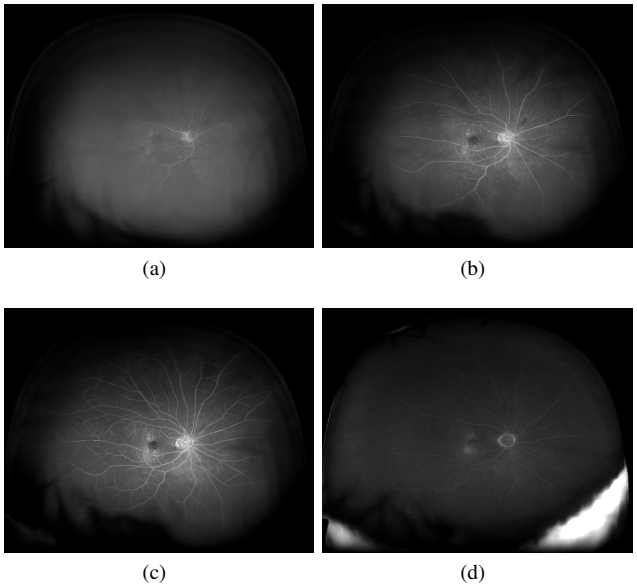

Fig. 1: Four frames corresponding to the 4 phases of a UWFV FA angiogram, showing up to 200° of the retina: (a) Arterial phase. (b) Arterio-venous phase. (c) Venous phase. (d) Late venous phase. (See high resolution images at http://vampire.computing.dundee.ac.uk)

Segmentation of UFWV FA images present various peculiarities. The main challenge is that, as the contrast dye perfuses the retina, different segments of the vasculature appear, so that the image content varies constantly. Occlusions due to eyelashes and eyelids may occur, as seen in Figure 1; some lesions might resemble vessels, creating false positives; and peripheral vessels often appear distorted and blurred.

The main contribution of this paper is the addition of a penalization step, run after vessel enhancement using steerable filters, in order to improve the segmentation of peripheral vessels and reduce the false positives on the region around the optic disc, choroidal circulation and lesion areas.

This paper is organized as follows: Section II describes our system. Section III detail the quantitative results of the segmentation. Finally, Section IV presents the discussion, conclusions and future work. All the material presented in this paper (an implementation of the algorithm, original images, ground truth and results) are publicly available at `http://vampire.computing.dundee.ac.uk`.

A. Perez-Rovira is with the School of Computing, University of Dundee (Scotland). `arovirez@computing.dundee.ac.uk`

K. Zutis is with the School of Computing, University of Dundee (Scotland). `kristszutis@computing.dundee.ac.uk`

J.P. Hubschman is with the Jules Stein Eye Institute, Los Angeles (USA). `hubschman@jsei.ucla.edu`

E. Trucco is with the School of Computing, University of Dundee (Scotland). `manueltrucco@computing.dundee.ac.uk`

978-1-4244-4122-8/11/$26.00 ©2011 IEEE

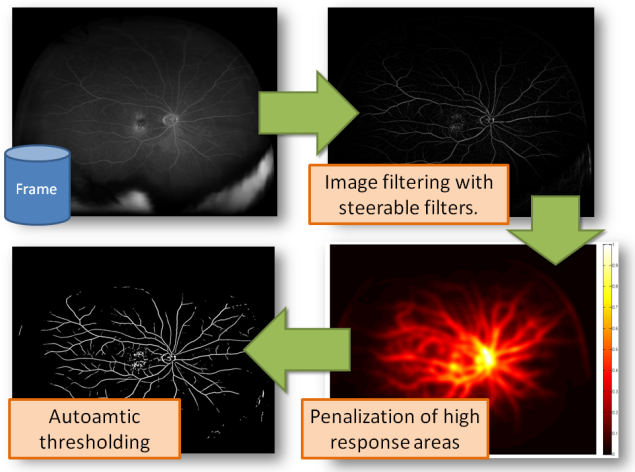

Fig. 2: Overview of the vessel segmentation system on UWFV FA images.

II. Methodology

A. Overview

Our system relies on 2-D steerable filters with closed-form expressions to detect ridges or edges on gray-scale images [9]. After enhancing tube-like structures, we add a penalization for areas with numerous strong responses in the enhanced image, in order to promote the extraction of isolated vessels in the periphery. Finally, automatic thresholding is applied by modeling the stability of the number of regions [10]. Figure 2 shows an overview of the system.

B. Image filtering with steerable filters

We use the implementation by Jacob *et al.* [9] in order to enhance the vessels in UWFV FA frames. The method is a general approach to 2D feature detection. A class of steerable functions is obtained from the optimization of a Canny-like criterion. The ridge detector is a re-interpretation of the ridge estimator based on the eigendecomposition of the Hessian matrix in terms of steerable filters. We use the second set of parameters suggested by Jacob *et al.* for the 4th-order filter to enhance ridges, only adjusting $\sigma = \delta/35$, where δ denotes the optic disc diameter. Vessel width in the retina are proportional to the optic disc diameter, and optic disc diameter is a near-constant measurement that can be easily obtained and used to tune the algorithm to images of different resolutions and fields of view.

Figure 3b shows an example of the response of a UWFV FA image to the steerable filter. The original image (Figure 1c) shows the optic disc in the centre, with the vasculature network emerging from it in a tree-like structure. A large white occlusion produced by the inferior eyelid and eyelashes is clearly visible at the bottom. A neovascularization lesion is visible above the macula (left of the optic disc). Notice the high density of enhanced vessels within this lesion and in the region surrounding the optic disc.

C. Penalization of high response areas

Detailed examination of UWFV FA images shows that peripheral vessels appear blurred, with weaker responses in the filtered image. At the same time, vessels around the optic disc have a stronger response as they appear more contrasted. Regions presenting choroidal circulation regions, and lesions with ridge-like textures (as the one present in the AMD sequence), present numerous pixels with relatively strong responses. Therefore, if a global threshold is applied, peripheral vessels might not have a strong enough response to be considered vessels and false positives can emerge around lesions, regions with choroidal circulation and around the optic disc, as shown in Figure 5b.

Consequently we decided to penalize regions with strong responses to promote the extraction of isolated vessels in the periphery and reduce false positives in noisy parts of the images. Somehow, this process can be regarded as a penalization of regions with high density of vessels with strong responses (i.e., around the optic disc, and thicker vessels), as shown in Figure 3, while promoting isolated vessels on the periphery.

In order to implement this idea, the response image obtained after applying the steerable filter, denoted as E, is smoothed using a $\delta \times \delta$ Gaussian window with a standard deviation of 2.5 pixels. The resulting image, E_s, highlights the regions with numerous strong responses (corresponding mainly to the optic disc and lesions). The penalized response image, E_p, is then computed as $E_p = E - E_s$.

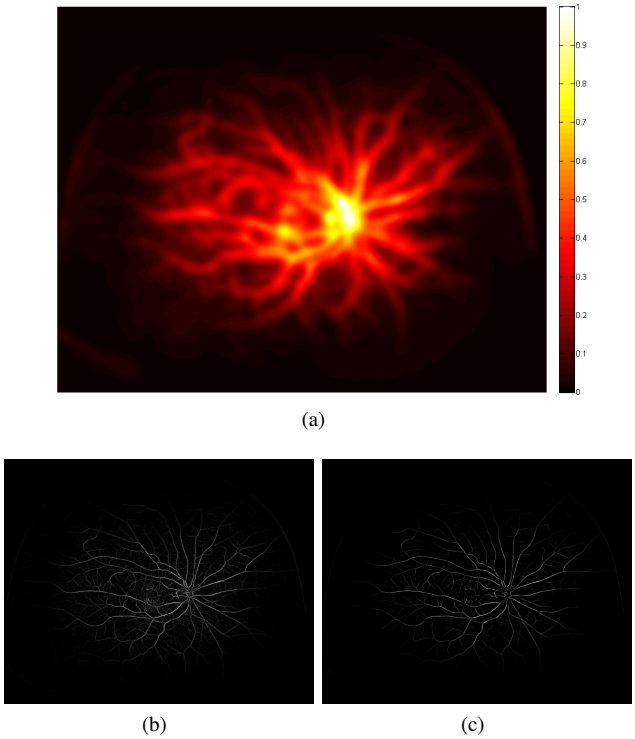

(a)

(b) (c)

Fig. 3: (a) High vessel response areas, E_s. (b) Response to the steerable filter before penalization, E. (c) Response to the steerable filter after penalization, E_p. (See high resolution images at http://vampire.computing.dundee.ac.uk)

D. Automatic thresholding

We now binarize E_p to achieve the vasculature map. We implemented an automatic global threshold algorithm based

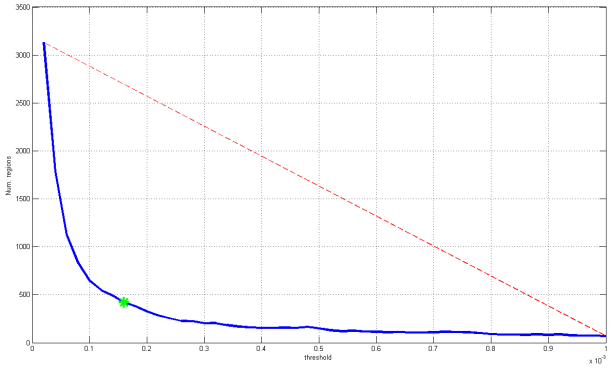

Fig. 4: Automatic threshold detection: Threshold values t_i on the x-axis and number of regions in $b(E_p, t_i)$ on the y-axis. The green asterisk is the further point from the straight line between t_i and t_I corresponding to the threshold value of 1.6×10^{-4}.

on the spatial distribution of the signal [10]. The location, size and number of vessel regions are unknown, but we expect that the application of increasingly higher thresholds will reduce progressively the number of regions. Specifically, at low threshold values there will be many disconnected regions caused mainly by noise; for increasing threshold values the number of regions will decrease. Moreover, high threshold values will yield fewer regions and the number of regions will be stable, dropping at a small rate. Consequently, the optimal threshold can be obtained by locating the interval of threshold values in which the number of regions stops decreasing fast and stabilizes.

Given this, we obtain a binary segmentation, B_i, from the penalized response image E_p using Equation (1).

$$B_i = b(E_p, t_i), \tag{1}$$

where t_i is the i-th threshold used and $i = [1, \ldots, I]$ with $I = 51$. We set $t_1 = 0$ and $t_I = 10^{-3}$. All t_i with $1 < i < I$ are evenly distributed between the minimum and maximum thresholds at steps of 2×10^{-5}. $b(E_p, t_i)$ is the function that binarizes E_p using the global threshold t_i: any pixel in E_p with a value greater than t_i will be 1, and 0 otherwise.

In order to select the optimum t_i we model $b(t_i)$ as an exponential decay (Figure 4). As predicted, the number of regions drop rapidly at low threshold values, caused by the many, noisy, disconnected regions. At high threshold values the number of regions becomes stable, decreasing at a slow rate. As suggested by Rosin *et al.* [10], a suitable partition point between the signal and noise is the "corner"of the curve, defined as the point of the curve with maximum deviation from the straight line between t_i and t_I, the s of the curve, Figure (4).

III. Results

In our experiments we used UWFV FA sequences of 3900×3072 frames acquired with an OPTOS P200C machine, courtesy of OPTOS plc [1]. The sequences contain between 10 and 15 frames acquired at irregular time intervals, capturing 200° of the retina. The data used includes two sequences: the AMD sequence shows a retina with age-related macula degeneration; the GER sequence shows a healthy retina.

TABLE I: Experimental results

	With penalization			*Without penalization*		
Frame	Pr	Rc	Ac	Pr	Rc	Ac
AMD1	0.4250	0.6940	0.9922	0.3786	0.6600	0.9911
AMD2	0.6007	0.7499	0.9813	0.5234	0.7369	0.9766
AMD3	0.7120	0.6681	0.9720	0.6567	0.5499	0.9657
AMD4	0.5886	0.3805	0.9690	0.4772	0.3280	0.9639
GER1	0.5769	0.6432	0.9930	0.5375	0.6424	0.9923
GER2	0.7450	0.5465	0.9721	0.6393	0.5550	0.9670
GER3	0.6929	0.4771	0.9540	0.6598	0.3443	0.9478
GER4	0.7157	0.5113	0.9773	0.6792	0.4919	0.9757
All	**0.6649**	**0.5510**	**0.9764**	**0.5945**	**0.4877**	**0.9725**

A close inspection of the segmentation (Figure 5) shows that the use of penalization of high response areas on the filtered image improves the segmentation, reducing notably the false positives in the central areas and segmenting a bigger portion of the vascular structure in the periphery. The binary mask computed without the penalization of high response areas shows artifacts around the main vessels. While the segmentation using density penalization shows fewer artifacts in the central part of the image, it still presents a large number of false positives in the part of the image corresponding to the eyelashes or eyelids skin, a region of the image of no clinical interest.

To evaluate quantitatively the segmentation results, one frame characteristic of each phase has been selected by the clinical author (JPH) in each sequence, giving a total of 8 frames. Binary vessel masks have been manually obtained from these frames (Figure 5a) to provide ground truth.

To measure the performance of our system, we use *Precision* (Pr), the fraction of correctly classified pixels as vessel among all the pixels classified as vessel; *Recall* (Rc), the fraction of correctly classified pixels as vessel among all the pixels that actually are vessel; and *Accuracy* (Ac), the portion of correctly classified pixels. The system achieves a precision of 0.6649, a recall of 0.5510 and an accuracy of 0.9764. Table I also shows the precision, recall and accuracy for each individual frame.

We repeated the experiments removing the penalization step, i.e., the binary segmentation is obtained by applying automatic thresholding directly on the response of the steerable filters. In this case, the precision decreases to 0.5945, the recall to 0.4877 and the accuracy to 0.9725. (Table I). The use of the penalization step increases the precision by 11.84%, the recall by 12.98% and the accuracy by 0.40%.

To study performance as a function of location, we computed precision, recall and accuracy in 6 different areas of the image. Region 1 is centered in the optic disc and has a radius of 300 pixels. Region 2 is a 200 pixels wide ring surrounding region 1. Region 3 to 6 are the subsequent 200 pixel wide rings. As a reference, the optic disc diameter in our data set is about 200 pixels. As seen in Figure 6, the use of a penalization step for areas with high vessel response

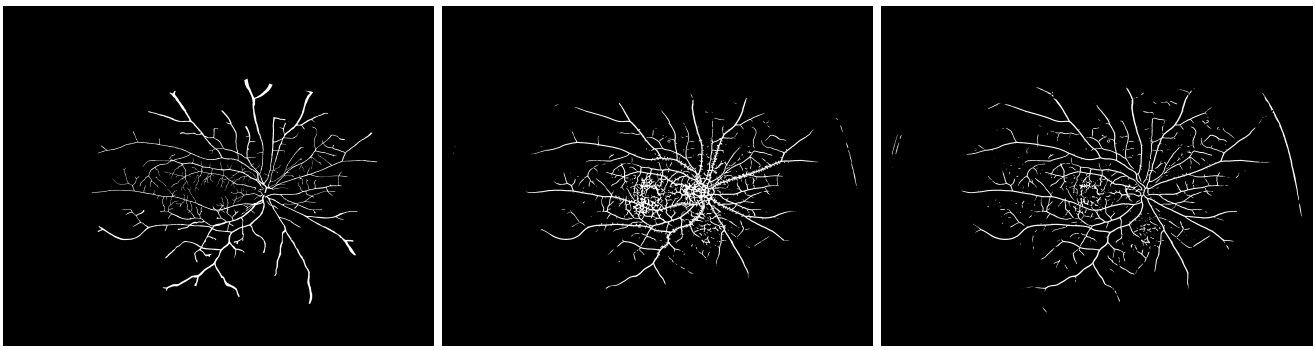

(a) (b) (c)

Fig. 5: (a) Ground truth for AMD2 (See figure 1b). (b) Vessel segmentation without the penalization step. (c) Vessel segmentation of our system. (See high resolution images at http://vampire.computing.dundee.ac.uk)

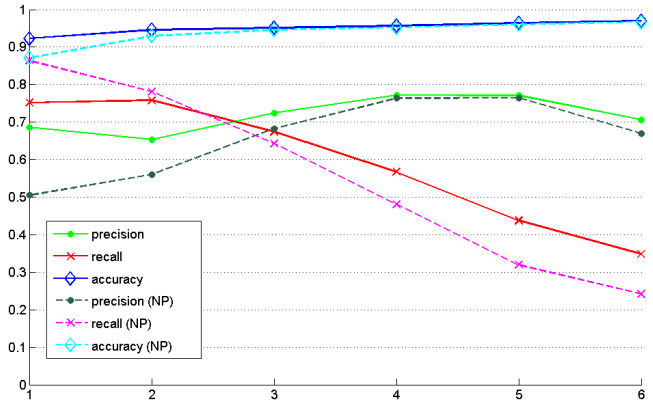

Fig. 6: Evaluation of the precision, recall and accuracy of the system at different regions for the 8 images. NP denotes the system without penalization of areas with high vesselness response.

increases the precision and accuracy of the system on the periphery and especially on the optic disc region and its surroundings (Regions 1, 2 and 3). It can be also observed that, without the penalization step, recall is much higher and precision lower in the regions close to the optic disc (1 and 2). This is because the system incorrectly considers most of the region as vessel (Figure 5b), forcing precision and accuracy to drop and recall to increase. In the periphery, the system with area penalization yields an increment on precision, recall and accuracy, indicating that more vessels are located correctly in those regions without generating a higher number of false positives.

The entire vessel segmentation process takes around 15 seconds on a Intel Core 2 Quad Q9400 at 2.67Ghz with 4GB of RAM.

IV. Discussion, Conclusions and Future Work

We have presented a system for locating vessels in UWFV FA frames based on the steerable filters and automatic thresholding. We have introduced a penalization step for regions with high vessel response to promote the extraction of peripheral vessels and at the same time increase the precision of the overall segmentation.

Our data and method are publicly available to facilitate further evaluation and comparisons and encourage the research on retinal image processing on UFWV FA sequences.

It is important to stress that recall, precision and accuracy are area measures, as they count the pixels and not the length of the vasculature network extracted (i.e. the number of vessels extracted). For instance, an algorithm that only detects the main vessels may yield a higher number of true positives than an algorithm that detects many thin vessels, as the area of thick vessels may be 4-5 times larger. Consequently, we plan further research on the use of non-area related metrics to evaluate better the quality of vessel segmentations.

References

[1] Optos plc. `http://www.optos.com/`.

[2] I. Tsui, A. Kaines, M.A. Havunjian, S. Hubschman, G. Heilweil, P.S. Prasad, S.C.N Oliver, F. Yu, E. Bitrian, J.P. Hubschman, T. Friberg, and S.D. Schwartz. Ischemic index and neovascularization in central retinal vein occlusion. *Retina*, 31:105–110, 2011.

[3] J.V.B. Soares, J.J.G. Leandro, R.M. Cesar, H.F. Jelinek, and M.J. Cree. Retinal vessel segmentation using the 2-D gabor wavelet and supervised classification. *Medical Imaging, IEEE Transactions on*, 25(9):1214–1222, 2006.

[4] C. Lupascu, D. Tegolo, and E. Trucco. FABC: retinal vessel segmentation using AdaBoost. *IEEE Transactions on Information Technology in Biomedicine*, 14(5):1267–1274, 2010.

[5] H.F. Jelinek, M.J. Cree, J. J.G. Leandro, J.V.B. Soares, R.M. Cesar, and A. Luckie. Automated segmentation of retinal blood vessels and identification of proliferative diabetic retinopathy. *Journal of the Optical Society of America A*, 24(5):1448–1456, 2007.

[6] M.E. Martinez-Perez, A.D. Hughes, S.A. Thom, A.A. Bharath, and K.H. Parker. Segmentation of blood vessels from red-free and fluorescein retinal images. *Medical Image Analysis*, 11(1):47–61, 2007.

[7] C.R. Buchanan and E. Trucco. Contextual detection of diabetic pathology in wide-field retinal angiograms. In *Engineering in Medicine and Biology Conference, 2008.*, pages 5437–5440, 2008.

[8] A. Perez-Rovira, E. Trucco, P. Wilson, and J. Liu. Deformable registration of retinal fluorescein angiogram sequences using vasculature structures. In *Engineering in Medicine and Biology Society*, pages 4383–4386, 2010.

[9] M. Jacob and M. Unser. Design of steerable filters for feature detection using canny-like criteria. *Pattern Analysis and Machine Intelligence, IEEE Transactions on*, 26(8):10071019, 2004.

[10] P. Rosin. Thresholding for change detection. In *Proceedings of the Sixth International Conference on Computer Vision*, ICCV '98, page 274281. IEEE Computer Society, 1998.